ground water

Rapid Communication/

Heated Distributed Temperature Sensing for Field Scale Soil Moisture Monitoring

by Arlen M. Striegl[1,2] and Steven P. Loheide II[3]

Abstract

Characterizing both spatial and temporal soil moisture (θ) dynamics at site scales is difficult with existing technologies. To address this shortcoming, we developed a distributed soil moisture sensing system that employs a distributed temperature sensing system to monitor thermal response at 2 m intervals along the length of a buried cable which is subjected to heat pulses. The cable temperature response to heating, which is strongly dependent on soil moisture, was empirically related to colocated, dielectric-based θ measurements at three locations. Spatially distributed, and temporally continuous estimates of θ were obtained in dry conditions ($\theta \leq 0.31$) using this technology (root mean square error [RMSE] = 0.016), but insensitivity of the instrument response curve adversely affected accuracy under wet conditions (RMSE = 0.050).

Introduction

Soil moisture is a key state variable in the hydrologic cycle, and is a primary factor governing soil-plant-atmosphere interactions and percolation through the vadose zone. Understanding spatial and temporal soil moisture dynamics on meter to kilometer scales is critical for understanding emergent hydrological and ecological processes on watershed and subwatershed scales (Robinson et al. 2008). Soil moisture conditions strongly affect precipitation recycling at continent scales (Entekhabi et al. 1996), rainfall-runoff responses at watershed scales (Dunne et al. 1970), and ecosystem structure, function, and diversity at subwatershed scales (Rodriguez-Iturbe and Porporato 2005).

Hydrologists are often interested in soil moisture monitoring at intermediate scales (subwatershed or catchment or vegetation stands), which often fall outside the scale of current measurement (i.e., time domain reflectometry, gravimetric sampling, and satellite remote sensing) capabilities (Robinson et al. 2008). Ground-based monitoring networks are generally composed of "point-in-space" or "point-in-time" measurements of volumetric water content (θ), while remote sensing methods provide estimates of θ with large spatial coverage, but poor spatial resolution (Schmugge et al. 2002). This inherent disconnect of spatial and temporal coverage makes it difficult to accurately characterize the spatial and temporal variability of subsurface hydrology at the site or field scale. Improved soil moisture measurements at these intermediate scales are needed for applications such as turf irrigation (Cardenas-Lailhacar et al. 2008), precision agriculture (Stafford 2000; Zhang et al. 2002), observing vertical movement of soil water that may lead to groundwater recharge, detecting leakage in landfill covers or liners (Khire et al. 1997), and hydroecological investigations (Robinson et al. 2008).

Transient heating methods have been used to estimate in situ soil heat capacity (Campbell et al. 1991), soil

[1]Department of Civil and Environmental Engineering, University of Wisconsin—Madison, 1415 Engineering Drive, 1269C Engineering Hall, Madison, WI 53706.

[2]Currently at Golder Associates Inc., Denver Office, 44 Union Boulevard, Lakewood, CO 80228.

[3]Corresponding author: Department of Civil and Environmental Engineering, University of Wisconsin—Madison, 1415 Engineering Drive, 1269C Engineering Hall, Madison, WI 53706; (608) 265-5277; fax: (608) 262-5199; loheide@wisc.edu

Received December 2011, accepted February 2012.

doi: 10.1111/j.1745-6584.2012.00928.x

thermal conductivity (de Vries 1952; Fritton et al. 1974; Bristow et al. 1994), water content (Bristow et al. 1993; Tarara and Ham 1997), and sap flow in plants (Cohen 1991). For a given in situ soil, thermal conductivity varies as a function of the ambient temperature and soil moisture. Within the range of normal environmental conditions, variations in soil thermal conductivity are primarily a function of the changes in θ (Olmanson and Ochsner 2006). By applying a constant power source to a resistance heating probe and measuring the induced temperature rise with respect to time, changes in θ can be estimated with calibrated single-probe heat pulse (SPHP) sensors (Shiozawa and Campbell 1990), because heat conduction away from the probe is affected by moisture-dependent, soil water bridges that form in pore throats and facilitate heat transfer between grains.

In recent years, commercially available distributed temperature sensing (DTS) has emerged as a very powerful environmental temperature sensing tool capable of high frequency (0.10 Hz) temperature measurements distributed along fiber optic cables in excess of 10 km in length with spatial resolutions as fine as sub 1 m (Selker et al. 2006). These measurement capabilities have allowed researchers to employ DTS in many unique hydrologic monitoring applications (Perzlmaier et al. 2006; Westhoff et al. 2007; Freifeld et al. 2008). Krzeminska et al. (2011) buried DTS fiber optic cables at multiple shallow depths to passively monitor soil moisture through near-surface soil temperature fluctuations due to diurnal radiative heating. Although this passive method of using DTS to measure soil moisture is advantageous because the low power requirements are ideal for remote study locations, difficulties arise in (1) placing the cables at consistent depths and spacing to accurately calculate thermal diffusivity (surrogate for θ) (Steele-Dunne et al. 2010) and (2) monitoring diurnal soil temperature fluctuations at depth because dense canopy and cloud cover limit induced temperature variation. Small-scale laboratory experiments have demonstrated the feasibility of an alternate, active approach for estimating θ using DTS technology in which a heat pulse is introduced from the cable itself and the resulting temperature response is monitored (Sayde et al. 2010).

The objective of this article is to outline the development and field deployment of a distributed θ sensing (DθS) system to monitor site scale, spatially distributed θ with high spatial and temporal resolution. In this approach, as with the SPHP sensor, a constant power source is applied to resistance heating elements bundled within the fiber optic cable sheathing. The resulting temperature response, which is a function of the moisture conditions surrounding the cable, is monitored over time with the fiber that act as distributed sensors. By examining this thermal response, and empirically relating it to dielectric θ measurements, spatially variable θ and process-based hydrologic phenomena such as wetting front dynamics and soil column drying can be observed over large spatial scales with high resolution.

Materials and Methods

Site Background

The study site is the Upper East Branch of the Pecatonica River Hydroecologic Observatory, which is located within the Driftless Area (Figure 1a) of southwestern Wisconsin, where the characteristic branching stream networks are bounded by deeply incised valleys and the landscape was left unglaciated during the Pleistocene. Overlying a gravel layer above the interface between bedrock and alluvial deposits is a silt-clay series that gradually grades into silt. These deposits are capped with a laminated silt loam representing cultural (caused by human activities) alluviation on the order of 30 to 400 cm over the last 200 years (Knox 1972, 2006). This cultural sediment deposition on the floodplain caused major hydrologic and ecologic regime shifts, prompting a novel restoration technique to re-establish the presettlement hydrologic dynamics and ecologic communities.

In 2006, The Nature Conservancy teamed with the Wisconsin Department of Natural Resources to remove the cultural sediment in an effort to reconstruct presettlement topography, decrease the depth to the water table, and to reintroduce wetland habitat (Booth et al. 2009). Once restoration was completed, a distinctive wet-dry-wet pattern developed along Transect AB, which can be seen from late-summer aerial photographs, where the wet regions are green, while the dry regions are brown (Figure 1b). The upper silt layer along Transect AB is relatively homogeneous and contains a sand fraction of 14% $\pm$ 5, a silt fraction of 82% $\pm$ 5, a clay fraction of 4% $\pm$ 1 and approximately 3% organic material. While the shallow soil did not vary substantially, the regions near the channel and near the margin of the floodplain remain much wetter due to groundwater upwelling, which is impeded by an underlying, low permeability layer in the central portion of the transect. The success of these restoration efforts in terms of re-establishing desired, native vegetation communities hinges on altering the soil moisture regimes to match the hydrologic niche of target species (Booth et al. 2012). A more complete description of the hydrostratigraphy, the hydrologic functioning, and the vegetative response to restoration at the site can be found in the studies by Booth et al. (2010, 2011, 2012). In this article, we apply the new DθS technology to describe the spatially variable θ regime of the upper homogeneous silt layer along Transect AB (DθS monitoring transect) that was re-exposed during restoration (Booth et al. 2010).

DθS Methods

DθS is an integrated system capable of making field-scale estimates of θ along a buried fiber optic cable with 2 m spatial resolution and 4 h temporal resolution. Similar to the SPHP sensor, generation of a uniform heat pulse from within the fiber optic cable, and along its entire length, causes the cable temperature to rise, which is measured along the cable using a DTS system. For homogeneous soil conditions such as those in the upper layer of our site, the temperature rise during heating is

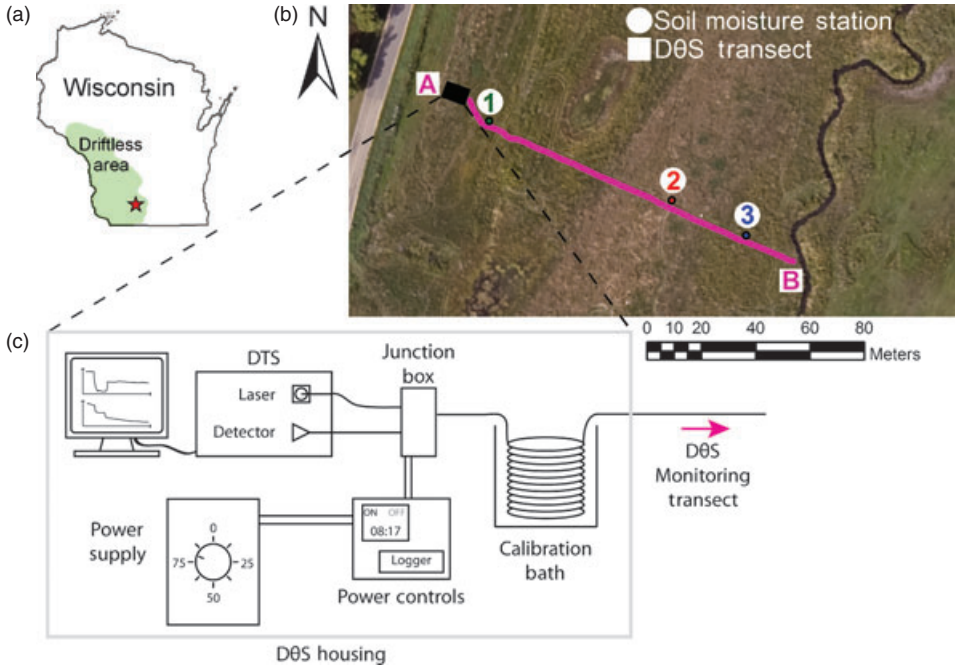

Figure 1. (a) Study site located in the Driftless Area of southwest Wisconsin within the floodplain of the Upper East Branch Pecatonica River. (b) Aerial photograph shows the DθS monitoring transect (AB) spanning three distinct hydrologic regimes. Stations 1 to 3 are continuously logging dielectric soil moisture sensors. (c) Schematic illustrates the equipment located within the environmentally controlled DθS housing used to monitor θ at a 20 cm depth along the DθS monitoring transect.

expected to be lesser in wet soils, and greater in dry soils due to the presence of more conductive pathways (i.e., water bridges between soil particles) and the greater heat capacity in wet soils. DθS is comprised of the following components: (1) a DTS system, (2) a fiber optic cable bundled with resistance heating wires and enclosed within a protective extrusion, (3) a variable transformer for resistance heating power supply, and (4) power control and timing instrumentation to provide consistent timing, duration, and intensity of heating intervals.

A DTS (Sensornet Ltd Halo DTS 4 km, BMP Enterprises, Houston, Texas) system with 2 m spatial resolution was used to measure temperature along the fiber optic cable at 20 s intervals throughout the duration of the study. The DTS accuracy is a function of the integration time and the cable length, and for this deployment with double-ended measurements, the estimated accuracy is 0.1°C (see Tyler et al. 2009 for a discussion of factors affecting accuracy). The cross section of the custom fiber optic cable bundle (fabricated by Gulf Coast Downhole Technologies, Houston, Texas) was designed to enhance the temperature response signal monitored by the DθS, while providing environmental protection to all components within the cross section. Approximately 45 m of fiber optic cable was submerged in an independently monitored water bath for DTS temperature calibration and validation purposes. An environmentally controlled (heating and cooling) enclosure was built on-site to house and protect the DθS and associated monitoring equipment (Figure 1c). To minimize soil disturbance, a vibratory plow (DitchWitch 100SX vibratory plow) was used on July 15, 2010 to knife the cable into the soil at a constant 20 cm depth along Transect AB, offset 1 m south of the θ monitoring stations. After installation, the transect was saturated by surface application of water and the gap that was created during installation was closed by applying pressure by foot. In addition, several natural precipitation events transpired prior to the study period to promote healing of the installation disturbance. A complete description of the installation process, including photos, can be found in the study by Striegl (2011).

Power was supplied to the resistance heating wires six times per day (every 4 h) for a minimum heating interval of 10 min each time, using a variable transformer (Variac 5021CT-2S, ISE Inc., Cleveland, Ohio) set to a constant output of 3.07 $\pm$ 0.005 W/m. Power supplied to the resistance heaters was controlled and monitored with a series of timers, mechanical contacts, and logging devices within the power control box. By applying a constant and uniform in time power supply pulse to the resistance heating wires within the fiber optic bundle, temporal changes and spatial variability in induced temperature responses can be primarily attributed to differences in θ.

Temperature measurements for the 5 min prior to the onset of each heating interval were averaged to determine the ambient temperature, T_o (°C), of each spatial unit of the cable, at time $t = 0$. The temperature rise above the ambient temperature after a specified time period was used to characterize response. The early time data were not included because they are largely a function of the thermal characteristics of the cable itself, and are minimally affected by the surrounding soil. Temperature measurements were averaged from $380 \leq t \leq 580$ s after the onset of heating to determine the temperature of the

cable after heating (T_{heat}). The difference between these two measurements was defined as the change in temperature due to induced heating after 480 s or 8 min ($\Delta T_8 = T_{heat} - T_o$).

Calibrating DθS with Traditional θ Measurements

The 130 m DθS monitoring transect was instrumented with three monitoring stations that continually logged θ using dielectric sensors (5TM Soil Moisture and Temperature sensors, Decagon Devices Inc., Pullman, Washington) at depths of 10 and 20 cm for DθS response calibration purposes. To capture the spatial and temporal trends in soil moisture distribution, the DθS (ΔT_8) response was obtained and empirically related to the independently collected soil moisture data sets from each monitoring station, which formed the DθS response curve. To generate this curve, soil moisture measurements obtained at Station 1 were related to the nearest (spatially and temporally) ΔT_8 measurements on the DθS cable. This process was repeated for Stations 2 and 3 and all data were combined to form a single DθS response curve.

Results and Discussion

DθS Temperature Responses

Volumetric soil moisture content estimates obtained from dielectric sensors ranged from 0.21 to 0.48 [−] over the study period (Figure 2a). Measurements of θ at Stations 2 and 3 were obtained at a 20 cm depth, consistent with the DθS monitoring cable depth, while θ at Station 1 was obtained from 10 cm depth due to sensor malfunction at the desired 20 cm depth. There existed only a minor vertical gradient in θ between 10 and 20 cm sensor depths at Stations 2 and 3 (mean difference in soil moisture of 0.011 [−] and mean absolute difference of 0.016 [−]), which supported the decision to substitute the 10 cm depth measurements for the missing 20 cm measurements at Station 1.

Station 2 experienced the driest conditions, whereas Station 3 experienced the wettest conditions (near saturation) throughout the study. Station 1 experienced the greatest temporal variability, while Station 2 exhibited slight variability and Station 3 exhibited virtually no variability. Booth et al. (2010, 2012) found that a variably continuous, silt-clay confining layer below the root zone that impedes groundwater upwelling was the major factor contributing to this spatial variation in θ conditions and the reduced temporal variation at Stations 2 and 3.

Spatially differential temperature rises of the DθS cable, due to variable θ conditions, were observed throughout the study period. An example temperature response taken by the DθS at each monitoring station on October 23, 2010 was extracted for illustrative purposes (Figure 2b). The temperature responses at each station are very similar for the first 60 s of the heating interval and are strongly controlled by the heat transfer properties of the cable. The late-time responses are controlled more by soil properties and therefore began to diverge due to

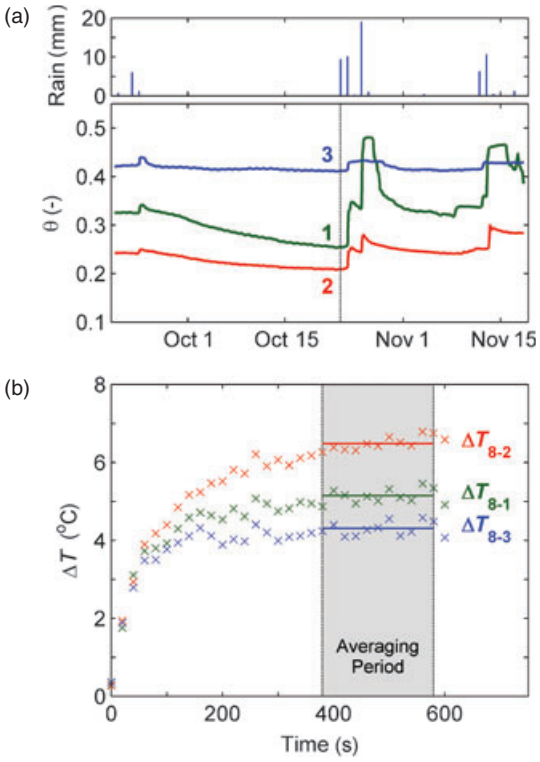

Figure 2. (a) Daily hyetograph and θ time series at Stations 1 to 3 for the duration of the study period. Measurements of θ at Stations 2 and 3 were obtained from dielectric θ sensors at a 20 cm depth, whereas θ at Station 1 was obtained from dielectric θ sensor at 10 cm. The gray vertical dotted line is the time of the sample DθS heating response in Figure 2b. (b) ΔT vs. time data obtained from the DθS at Stations 1 to 3 on October 23, 2010 at 00:00. ΔT_8 was obtained by averaging ΔT measurements over the interval $380 \leq t \leq 580$ s. Note that the number in the subscript of ΔT_8 is the station number.

the spatially variable θ conditions. As expected, Station 2 (driest) experienced the largest temperature response (ΔT_8) due to heating. Station 3 was the wettest and experienced the most muted temperature response, while the Station 1 response was intermediate. Examining the relationship between changes in ΔT_8 and changes in θ in Figure 2b, a small change in θ between Stations 1 and 2 caused a relatively large change in the ΔT_8 response. In contrast, a relatively large change in θ between Stations 1 and 3 resulted in a small change in the ΔT_8 response, suggesting decreased sensitivity in the ΔT_8 response under wetter conditions.

DθS Calibration

Spatially distributed, temporally continuous estimates of θ were obtained by empirically relating DθS measurements of ΔT_8 to colocated, dielectric measurements of θ at Stations 1 to 3 (Figure 3a). The slope of the ΔT_8-θ relationship (DθS response curve) decreased with increasing θ, further suggesting decreased sensitivity at higher soil moisture contents, which is consistent with findings from previous studies (Weiss 2003; Sayde et al. 2010). While fitting a biexponential function to the ΔT_8-θ

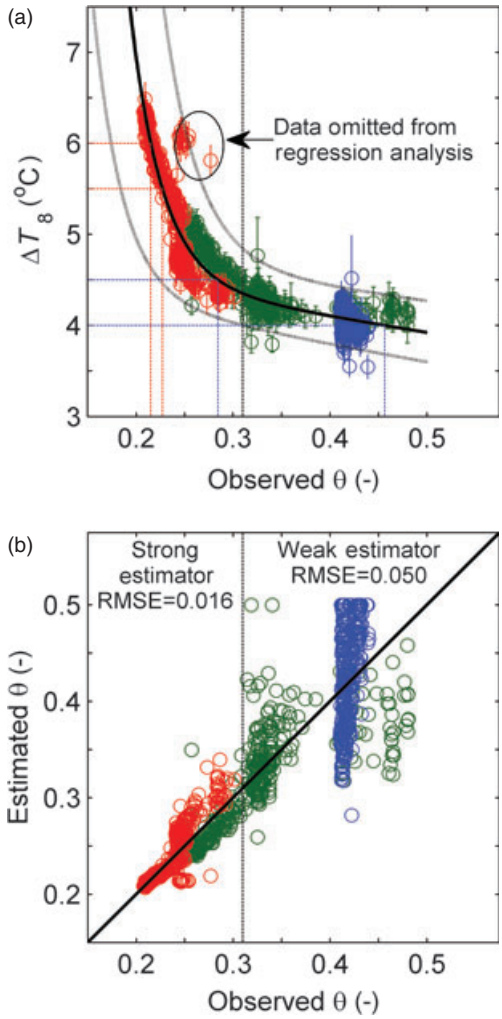

Figure 3. (a) DθS response curve empirically relating DθS measurements of ΔT_8 to colocated dielectric measurements of θ, with the gray lines indicating the 95% confidence level for the relationship. The green, red, and blue data points were obtained from Stations 1, 2, and 3, respectively. (b) DθS estimated θ vs. observed θ for the study period at the three monitoring stations.

relationship using least squares regression ($\Delta T_8 = 1109 \exp[-30.56\ \theta] + 4.891 \exp[-0.4412\ \theta]$); a subset of data (13 of 316 points) were omitted because of the effects of spatially variable wetting front dynamics. The omitted points all occurred at Station 2 immediately following the October 24 rain event, which will be discussed further in the following section. The coefficient of determination and root mean square error (RMSE) of the fitted function are 0.9397 and 0.16°C, respectively. Because the regression equation is specific to this DθS cable and site soil, variations in cable cross section, material thermal properties, or soil texture and density would cause a different response to heating, requiring a new response curve.

Soil moisture was estimated at each monitoring station location through time from DθS-derived measurements of ΔT_8, using the resulting DθS response curve (Figure 3b). Estimates of θ were limited to $\theta \leq 0.50$ [−] in order to constrain the biexponential function on the wet end of the DθS response curve. Repeatable and distinct estimates of θ were obtained in the strong estimator region ($\theta \leq 0.31$), which demonstrates a reasonable accuracy (RMSE = 0.016 [−]) and negligible bias (mean error = −0.00025 [−]) based on 488 data points. On the contrary, estimates of θ above 0.31 [−] were less accurate but still unbiased (RMSE = 0.050 [−], mean error = −0.0033 [−]) based on 565 data points, due to the low sensitivity of DθS measurements in wet conditions. It is interesting to note that in the range of 0.25 to 0.30, where data from sensors 1 and 2 overlap, there is an apparent difference in the response curves. This relatively slight difference could be an indication of the degree to which slight soil textural differences affect the calibration relationships at different locations; it could be an indication of hysteresis since these data points are among the driest collected from sensor 1 and the wettest from sensor 2; or it could be an artifact of the cable and the sensor at Station 1 being installed at different depths.

Site θ Dynamics and Discussion

Spatially and temporally distributed measurements of the DθS thermal response throughout the study period can be seen in the ΔT_8 transect time series (Figure 4a). The dimensions of each pixel in the ΔT_8 transect time series are equal to the temporal resolution of measurements, which was 4 h (x axis), by the spatial resolution of measurements, which was 2 m (y axis). The red colors represent a greater temperature rise, and therefore drier conditions. Using the ΔT_8 transect time series and the DθS response curve, θ at 20 cm depth was estimated at every location along the DθS monitoring transect throughout the study period (Figure 4b). Although moisture conditions were spatially and temporally variable, the central zone ($50 \leq y \leq 92$ m) was the driest (reds), and the near-stream zone ($98 \leq y \leq 122$ m) was the wettest (blues) throughout the study period. Each rainfall event caused spatially differential wetting of the soil column depending on the antecedent moisture conditions and the connection with shallow groundwater. This wetting phenomenon is seen with the sudden jumps from red to blue on the following dates: October 23 and 27, 2010 and November 7, 2010. The lack of rainfall from September 24 through October 23 led to a substantial drying of the DθS monitoring transect, except for zones known to have a strong connection with shallow groundwater (i.e., $98 \leq y \leq 122$ m). The drying phenomenon exhibits a more gradual transition from wet to dry (blue to red), similar to the trends seen in the θ time series (Figure 2a). The observed jump for a wetting front and the subsequent gradual drying are both functions of pore-scale water movement and plant water use. A snapshot of estimated θ along the entire transect was taken on October 25, 2010. This snapshot compared well with nine gravimetric and three dielectric measurements of θ distributed across the monitoring transect (Figure 4c), demonstrating that the DθS system can capture spatial patterning in moisture conditions.

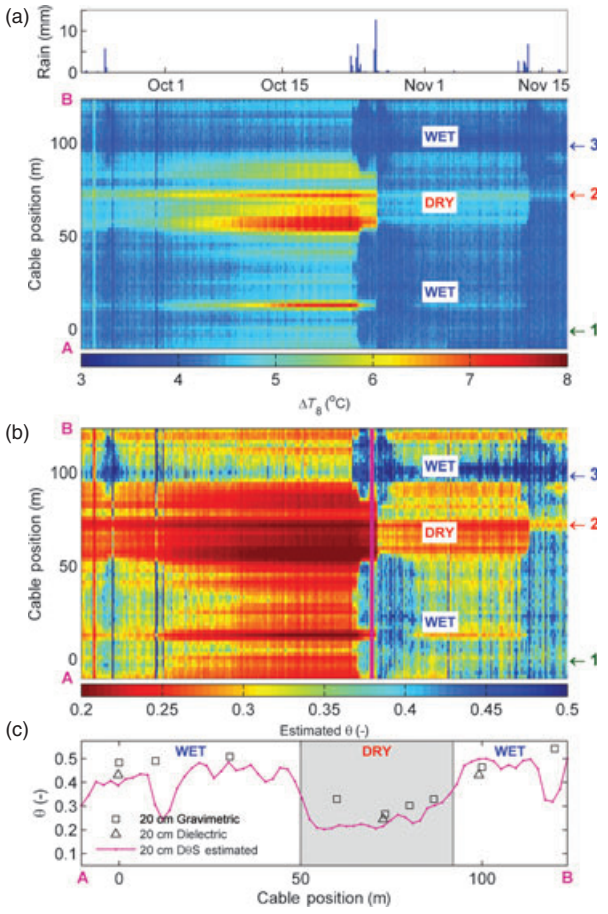

Figure 4. (a) Rainfall on a 4-h interval and measured ΔT_8 profile time series along DθS transect throughout the study period. Each pixel is equal to 4 h in the x-direction and 2 m in the y-direction. Reds represent drier conditions. (b) Estimated θ profile time series along DθS transect throughout the study period, generated from the ΔT_8 profile time series. (c) A snapshot in time of the soil moisture transect (shown as the magenta line in Figure 4b) showing gravimetric θ samples, dielectric θ measurements at Stations 1 to 3 and DθS predicted θ on October 25, 2010 at 16:00.

The greatest drying occurred in the central zone, with θ approaching 0.20. Consecutive rainfall events from October 24 to 26, 2010 caused all of the DθS monitoring transect to reach saturated (blue) conditions except the dry, central zone. Prior to the October 24 to 26 precipitaiton event, there was approximately 4 to 6 cm of fillable pore space in the upper 20 cm at Station 2, but precipitation of 2.0 cm on October 24 to 25 was slightly less than would be required to completely wet the soil. It was not until after an additional 1.9 cm of precipitation on October 26 that the wetting front reached the cable depth in the central zone (~3 d after the rest of the DθS transect). Because the dry zone had sufficient fillable pore space in the upper 20 cm, infiltration from the first rainfall events did not exceed this storage capacity, which was the reason for the differential depth of wetting front propagation. The wetting front reached the dielectric θ sensor at Station 2 after the first set of rainfall events from October 24 to 25, while the DθS cable, separated horizontally by one meter, did not detect the wetting front until days later, following additional rainfall. The depth of penetration of the wetting front was likely very near the depth of the cable, and slight discrepancies in the installation depth and fingering phenomena at the wetting front may have contributed to this observed difference in soil moisture dynamics. Because the DθS and θ sensor at Station 2 were not experiencing the same moisture conditions during this time period, this subset of data was omitted during the least squares regression analysis to develop the DθS response curve relating ΔT_8 to θ (Figure 3a), which was first discussed in the previous section.

Discussion of Errors

One source of error with the DθS method stems from the insensitivity in the flat (wet) region of the DθS response curve. In the dry region, where ΔT_8 is a strong estimator, a small error in measured ΔT_8 ($\sigma_{\Delta T_8}$) will cause small errors (σ_θ) in estimated θ (i.e., $\sigma_{\Delta T_8}$ =0.5°C causes $\sigma_\theta = 0.012$ [−]). Conversely, in the wet region, where ΔT_8 is a weak estimator, a small error in measured ΔT_8 will cause large errors in estimated θ (i.e., $\sigma_{\Delta T_8}$ =0.5°C causes σ_θ =0.172 [−]). Because of this limitation, which is inherent in the measurement technique, the estimating power of the DθS decreases for θ>0.31 [−] for the soil studied here.

The Halo DTS is not a unit typically used for remote environmental applications because of its sensitivity to fluctuations in ambient temperature and relative humidity. Systematic errors arose during field deployment due to abrupt housing temperature fluctuations that caused the DθS unit to experience rapid, and likely differential, changes in temperature. During these times, the recorded data sets became contaminated, necessitating the filtering process outlined in the appendix. As a result of this data filtering, 10% of the 351 ΔT_8 traces were discarded. In future deployments, additional insulation should be placed around the DθS unit to buffer against these rapid temperature changes within the housing.

While the vibratory plow method of fiber burial minimized soil structure disturbance, it still likely altered macropore structures. This disturbance may have changed the pathways through which water infiltrates into the soil and reaches the 20 cm cable depth. This may have also altered the conductive pathways through which heat conducts away from the cable during a heat pulse. Consideration of proper cable installation is necessary to achieve undisturbed monitoring conditions.

Future research is needed to determine how to improve on the DθS system developed here and improve performance across a range of soil types. Additional research would help to optimize hybrid cable configurations, heating schemes, and interpretation strategies for DTS-based heating methods. Streamlined calibration methods that determine the resulting accuracy under heterogeneous soil textural conditions along the cable would result in a more robust and widely applicable method. Improvements to cable installation (burial) and guidelines for a range of field conditions would bolster the utility

and accuracy of the method, making it more attractive to researchers who study vadose zone hydrology.

Conclusion

This study has demonstrated that DθS shows great promise for spatially and temporally characterizing θ dynamics in a site-scale field deployment, especially in moderate to dry conditions. The DθS-measured temperature rise above ambient temperature (ΔT_8), after 8 min of axial heating from within the fiber optic cable, was found to be a strong estimator of soil moisture in dry conditions ($\theta \leq 0.31$ [−]) at this site. For $\theta \leq 0.31$ [−], the RMSE between estimated and observed θ was 0.016 [−], while the RMSE for $\theta > 0.31$ [−] (wet conditions) was 0.050 [−]. This novel method for monitoring site-scale moisture conditions could find application in hydroecological studies, turf management, precision agriculture, and detection of groundwater recharge or leakage through landfill liners.

Acknowledgments

This material is based on work supported by the National Science Foundation under Grant CBET-0954499. Funding for this research was also provided by the Arthur H. Frazier Fellowship. Any opinions, findings, conclusions, or recommendations expressed in this material are those of the author(s) and do not necessarily reflect the views of the funding agencies. We would like to thank Steve Richter of The Nature Conservancy and Bob Hansis from the Wisconsin Department of Natural Resources for their enthusiastic support and interest in the research, as well as the following individuals for helpful discussions and/or logistical field support during the research effort: Eric Booth, Gerard Kluitenberg, Chris Lowry, Eric Mark, and Matt Weber. We would also like to thank two anonymous reviewers for the helpful and expedited reviews of this article.

Appendix: Data Filtering and Removal

Initially, unexplained, abrupt variations from the trend in measured ΔT_8 were observed at random times during the study period. It was determined that rapid changes in DθS unit temperature (T_{unit}), which occurred when the air conditioner blew cool air directly onto the unit, were causing "ghost" spikes in temperature readings along the cable that were not indicative of real temperature changes. These "ghost" spikes occurred in the buried portions of the cable, in the portion of the cable embedded in the distributed temperature sensing (DTS) unit itself, and in the calibration bath, which maintained a relatively constant temperature. It is assumed that when components of the DTS changed rapidly in temperature, the measured DTS temperature shifted, causing the erroneous "ghost" spikes at all measurement locations. A linear function was fit to the T_{unit} time series data during a window period of 5 min before and after each heating interval ($-5 \leq t \leq +15$ min) using least squares regression. The root mean square difference (RMSD) between the observed T_{unit} and the regression for each heating interval was calculated to detect periods of rapid and nonlinear temperature changes. For the cases where the RMSD exceeded a predefined threshold ($RMSD_{thresh} \geq 0.08$), the data from that particular heating interval were considered to be contaminated by the rapid fluctuations in T_{unit}, and therefore all data from that time were discarded. Of the 351 data points in time examined during the study period, 35 (10%) were discarded on the basis of exceeding the RMSD threshold. Many days did not require data exclusions; however, for those days that did, the maximum number of ΔT_8 traces discarded during a given day was two out of six measurements taken. The discarded data points were then estimated using linear interpolation between the heating intervals preceding and following the excluded data point. This method of data filtering eliminated any effects these "ghost" spikes in temperature readings were having on the estimates of θ.

References

Booth, E.G., and S.P. Loheide. 2012. Hydroecological model predictions indicate wetter and more diverse soil water regimes and vegetation types following floodplain restoration. *Journal of Geophysical Research - Biogeosciences.* DOI: 10.1029/2011JG001831.

Booth, E.G., and S.P. Loheide II. 2011. Comparing surface effective saturation and depth-to-water-level as predictors of plant composition in a restored floodplain wetland. *Ecohydrology 4.* DOI: 10.1002/eco.250.

Booth, E.G., and S.P. Loheide II. 2010. Effects of evapotranspiration partitioning, plant water stress response and topsoil removal on the soil moisture regime of a floodplain wetland: Implications for restoration. *Hydrological Processes* 24, no. 20: 2934–2946. DOI: 10.1002/hyp.7707.

Booth, E.G., S.P. Loheide II, and R.I. Hansis. 2009. Postsettlement alluvium removal: A novel floodplain restoration technique (Wisconsin). *Ecological Restoration* 27: 136–139. DOI: 10.3368/er.27.2.136.

Bristow, K.L., R.D. White, and G.J. Kluitenberg. 1994. Comparison of single and dual probes for measuring soil thermal-properties with transient heating. *Australian Journal of Soil Research* 32, no. 3: 447–464.

Bristow, K.L., G.S. Campbell, and K. Calissendorff. 1993. Test of a heat-pulse probe for measuring changes in soil-water content. *Soil Science Society of America Journal* 57, no. 4: 930–934.

Campbell, G.S., C. Calissendorff, and J.H. Williams. 1991. Probe for measuring soil specific-heat using a heat-pulse method. *Soil Science Society of America Journal* 55, no. 1: 291–293.

Cardenas-Lailhacar, B., M.D. Dukes, and G.L. Miller. 2008. Sensor-based automation of irrigation on bermudagrass, during wet weather conditions. *Journal of Irrigation and Drainage Engineering-Asce* 134, no. 2: 120–128. DOI: 10.1061/(asce)0733-9437(2008)134:2(120).

Cohen, Y. 1991. Determination of orchard water requirement by a combined trunk sap flow and meteorological approach. *Irrigation Science* 12, no. 2: 93–98.

de Vries, D. 1952. A nonstationary method for determining thermal conductivity of soil in situ. *Soil Science* 73: 83–89.

Dunne, T., and R.D. Black. 1970. An experimental investigation of runoff production in permeable soils. *Water Resources Research* 6, no. 2: 478–490.

Entekhabi, D., I. Rodriguez Iturbe, and F. Castelli. 1996. Mutual interaction of soil moisture state and atmospheric processes. *Journal of Hydrology* 184, no. 1–2: 3–17.

Freifeld, B.M., S. Finsterle, T.C. Onstott, and P. Toole. 2008. Ground surface temperature reconstructions: Using in situ estimates for thermal conductivity acquired with a fiber-optic distributed thermal perturbation sensor. *Geophysical Research Letters* 35, no. 14: 1–5 DOI: L1430910.1029/2008gl034762.

Fritton, D., W. Busscher, and J. Alpert. 1974. An inexpensive but durable thermal conductivity probe for field use. *Soil Science Society of America Proceedings* 38: 854–855.

Khire, M.V., C.H. Benson, and P.J. Bosscher. 1997. Water balance modeling of earthen final covers. *Journal of Geotechnical and Geoenvironmental Engineering* 123, no. 8: 744–754. DOI: 10.1061/(ASCE)1090-0241(1997)123:8(744).

Knox, J.C. 2006. Floodplain sedimentation in the Upper Mississippi Valley: Natural versus human accelerated. *Geomorphology* 79, no. 3–4: 286–310. DOI: 10.1016/j.geomorph.2006.06.031.

Knox, J.C. 1972. Valley alluviation in southwestern Wisconsin. *Annals of the Association of American Geographers* 62: 401–410.

Krzeminska, D.M., S.C. Steele-Dunne, T.A. Bogaard, M.M. Rutten, P. Sailhac, and Y. Geraud. 2011. High-resolution temperature observations to monitor soil thermal properties as a proxy for soil moisture condition in clay-shale landslide. *Hydrological Processes 25.* DOI:10.1002/hyp.7980.

Olmanson, O.K., and T.E. Ochsner. 2006. Comparing ambient temperature effects on heat pulse and time domain reflectometry soil water content measurements. *Vadose Zone Journal* 5, no. 2: 751–756. DOI: 10.2136/vzj2005.0114.

Perzlmaier, S., K. Straber, T. Strobl, and M. Aufleger. 2006. Integral seepage monitoring on open channel embankment dams by the DFOT heat pulse method. In *74th Annual Meeting, International Committee on Large Dams.* Spain: Barcelona.

Robinson, D.A., C.S. Campbell, J.W. Hopmans, B.K. Hornbuckle, S.B. Jones, R. Knight, F. Ogden, J. Selker, and O. Wendroth. 2008. Soil moisture measurement for ecological and hydrological watershed-scale observatories: A review. *Vadose Zone Journal* 7, no. 1: 358–389. DOI: 10.2136/vzj2007.0143.

Rodriguez-Iturbe, I., and A. Porporato. 2005. *Ecohydrology of Water-Controlled Ecosystems: Soil Moisture and Plant Dynamics.* Cambridge, UK: Cambridge University Press.

Sayde, C., C. Gregory, M. Gil-Rodriguez, N. Tufillaro, S. Tyler, N. van de Giesen, M. English, R. Cuenca, and J.S. Selker. 2010. Feasibility of soil moisture monitoring with heated fiber optics. *Water Resources Research* 46, no. 8. DOI: W0620110.1029/2009wr007846.

Schmugge, T.J., W.P. Kustas, J.C. Ritchie, T.J. Jackson, and A. Rango. 2002. Remote sensing in hydrology. *Advances in Water Resources* 25, no. 8–12: 1367–1385.

Selker, J.S., L. Thevenaz, H. Huwald, A. Mallet, W. Luxemburg, N.V. de Giesen, M. Stejskal, J. Zeman, M. Westhoff, and M.B. Parlange. 2006. Distributed fiber-optic temperature sensing for hydrologic systems. *Water Resources Research* 42, no. 12. DOI: W1220210.1029/2006wr005326.

Shiozawa, S., and G.S. Campbell. 1990. Soil thermal conductivity. *Remote Sensing Reviews* 5, no. 1: 301–310.

Stafford, J.V. 2000. Implementing precision agriculture in the 21st century. *Journal of Agricultural Engineering Research* 76, no. 3: 267–275.

Steele-Dunne, S.C., M.M. Rutten, D.M. Krzeminska, M. Hausner, S.W. Tyler, J. Selker, T.A. Bogaard, and N.C.V. de Giesen. 2010. Feasibility of soil moisture estimation using passive distributed temperature sensing. *Water Resources Research* 46, no. 12. DOI: W0353410.1029/2009wr008272.

Striegl, A.M. 2011. Development and field implementation of a distributed soil moisture sensor using heated fiber optics. M.S. thesis, University of Wisconsin—Madison, Madison, Wisconsin.

Tarara, J.M., and J.M. Ham. 1997. Measuring soil water content in the laboratory and field with dual-probe heat-capacity sensors. *Agronomy Journal* 89, no. 4: 535–542.

Tyler, S.W., J.S. Selker, M.B. Hausner, C.E. Hatch, T. Torgersen, C.E. Thodal, and S.G. Schladow. 2009. Environmental temperature sensing using Raman spectra DTS fiber-optic methods. *Water Resources Research* 45: W00D23. DOI: 10.1029/2008WR007052.

Weiss, J.D. 2003. Using fiber optics to detect moisture intrusion into a landfill cap consisting of a vegetative soil barrier. *Journal of the Air and Waste Management Association* 53, no. 9: 1130–1148.

Westhoff, M.C., H.H.G. Savenije, W.M.J. Luxemburg, G.S. Stelling, N.C. van de Giesen, J.S. Selker, L. Pfister, and S. Uhlenbrook. 2007. A distributed stream temperature model using high resolution temperature observations. *Hydrology and Earth Systems Science* 11, no. 4: 1469–1480.

Zhang, N.Q., M.H. Wang, and N. Wang. 2002. Precision agriculture-a worldwide overview. *Computers and Electronics in Agriculture* 36, no. 2–3: 113–132.